Unsteady Performance of a Mixed-flow Turbine with Nozzled Twin-entry Volute Confronted by Pulsating Incoming Flow

Yingxian Xue[1], Mingyang Yang [1*], Ricardo F. Martinez-Botas[2], Bijie Yang[2], Kangyao Deng[1]

1. Shanghai Jiao Tong University, Shanghai 200240, China
2. Imperial College London, London SW72AZ, UK

Abstract

Turbine with twin-entry volute has advantage of utilizing energy from pulsatile exhaust gas and improving low-speed torque of an internal combustion engine. This paper investigates unsteady performance of a mixed flow turbine with nozzled twin-entry volute confronted by pulsatile incoming flow. The turbine performance at pulsating conditions with different Strouhal numbers (St) is studied via experimentally validated numerical method. Results show that the unsteadiness of turbine performance is enhanced as Strouhal number increases. In particular, the cycle-average efficiency at St=0.522 is about 3.4% higher than that of quasi-steady condition (St=0). Instantaneous loss breakdown of the turbine shows that the entropy generation rate of turbine components reduces evidently at pulsating conditions as Strouhal number increases, especially for the nozzle. Specifically, the cycle-averaged reduction of the loss in the nozzle is 37.3% at St=0.522 compared with that of St=0. The flow analysis shows that secondary flow which contributes to the majority of loss in the nozzle, including flow separation, horseshoe vortex, and reversed flow near the leading edge, are notably alleviated as Strouhal number increases. The alleviation of the flow structures are resulted from two reasons: one is that the flow distortion at the nozzle inlet is evidently depressed by the pulsating conditions,

* *Corresponding author – myy15@sjtu.edu.cn*

the other is that the inertia of the low momentum flow in the nozzle damps flow evolution at pulsating incoming flow. Consequently, the loss is reduced and the turbine performance is benefited by the pulsating inflows.

Keywords: Turbine; Twin-entry volute; Pulsating conditions; Unsteady performance;

Nomenclatures

CFD	Computational Fluid Dynamic	
C_p	Specific heat	J/(kg·°C)
f	Pulse frequency	Hz
L	Characteristic length	m
MFP	Mass flow rate parameter	kg/s·√K/Pa
m	Mass flow rate	kg/s
P	Pressure	Pa
PR	Pressure ratio	-
St	Strouhal number	-
T	Temperature	K
U	Characteristic velocity	m/s
UAV	Unmanned aerial vehicle	

Greek letters

η	Efficiency	-
μ	Dynamic viscosity	Pa·s
μ_t	Turbulence viscosity	Pa·s
τ	Torque	N·m
τ_{ij}	Shear stress tensor	Pa
σ	Entropy generation rate	W/K

ω	Rotation velocity	rad/s

Subscripts

act	Actual
cyc	Cycle-average value
equi	Equivalent
hub	Limb near hub
inst	Instantaneous value
is	Isentropic
i	Component in the *i* direction
j	Component in the *j* direction
s	Static
shr	Limb near shroud
t	Total

Introduction

Turbocharging is the key technology enabling high-altitude operation of internal combustion engine for long-endurance unmanned aerial vehicle (UAV) [1]. The performance of turbocharger turbine which extracts exhaust energy from cylinders for boosting fresh air has strong impact on the altitude adaptability of the turbocharged engine. For a multi-cylinder engine, especially for 4/6 cylinders, the exhaust manifold is normally grouped into two limbs in order to separate pulses of exhaust gas and hence avoid interference of breathing among cylinders. Correspondingly, there are two entries in the volute of turbocharger turbine for the configuration of such exhaust manifold. For the turbine with twin-entry volute, the exhaust pulse can be well reserved in each limb and turbocharged engine has remarkable advantage of the low-speed torque and transient performance [2, 3], thus enables good performance of manoeuvrability. However, due to the different timing of pulses in two limbs, the twin-entry

volute is always confronted by two streams of pulsating exhaust gas which are always at different phases. Consequently, the admission condition of the turbine changes continuously in time in wide range during a pulse period. How the turbine with twin-entry volute behaves under the highly unsteady condition consisted of two out-of-phase pulses needs to be studied in details in order to enlighten performance improvement of the turbine.

Experimental and numerical investigations have been carried out on the performance and flow field of the twin-entry turbine at steady conditions [4-8]. The swallowing capacity and efficiency are dramatically different between the full admission and unequal admissions. Moreover, the performance is found moderately different between the admissions in the two limbs. The flow patterns at volute exit are considered to be the main reasons for the discrepancies. Compared with the researches at steady conditions, few investigations have been reported which focus on the unsteady performance of twin-entry turbine confronted by pulsating incoming flow. Romagnoli experimentally investigated the performance of a twin-entry turbine at unsteady conditions in terms of in-phase and out-of-phase pulses [9]. It is found that the performance is highly related to the pulse frequency. Specifically, the cycle averaged efficiency is not monotonically depended on the frequency for both unsteady cases. No further discussions on the reason for the performance enhancement at pulsating condition have been given in the literature. It is worth mentioning that the magnitude of the pulse is coupled with the frequency in the experiment. Therefore, the influence of frequency on the turbine performance is in fact contributed by both the frequency and the pulse magnitude. For the single-entry turbine, comprehensive experimental and numerical investigations have confirmed that the performance of the turbine is more likely to deteriorate at pulsating conditions [10, 11]. Comprehensive researches have been carried out by Copeland and Newton on a double-entry turbine, of which the volute passage is divided into two limbs in circumferential direction, at both steady and pulsating conditions [12-14]. Similar to the phenomenon in a single-entry

turbine, the performance of this type of two-entry turbine deteriorates evidently as the pulse frequency increases. Highly unsteady flow distortion in circumferential direction at the inlet of the rotor and nozzle is concluded to contribute to the unsteady effect. However, for a twin-entry turbine, because the volute passage is divided into two limbs in axial direction, the flow at the exit of the volute is highly distorted in spanwise of the rotor inlet at pulsating conditions [15, 16]. The flow mechanism for the performance unsteadiness caused by the pulsating condition in a twin-entry turbine is expected to be profoundly different from that in either the double-entry or single-entry turbine. In order to enlighten the design methodology/flow control method of a turbine to enhance its performance, it is valuable to obtain the knowledge of the unsteadiness of turbine performance with twin-entry volute at pulsating conditions.

This paper studies the performance of a mixed flow turbine with a twin-entry nozzled volute under pulsating inflows via the experimentally validated numerical method. The paper is organized in three main sections. Firstly, the numerical method is introduced and experimentally validated at pulsating conditions. Following that, performance of the turbine is compared and analyzed at different pulsating conditions. In the last section, detailed flow field is studied to understand the mechanism of the unsteady performance.

Numerical Method and Validation

A mixed-flow turbine with twin-entry nozzled volute developed by Imperial College London is investigated in this paper. The ratio of throat area and the radius of its center of the volute, referring as A/R, is 33mm. There are 15 leaned vanes in the nozzle and the vane angle in this paper is set as 60 degrees (the maximum efficiency can be achieved by this angle). A divider is inserted in the middle of the volute to divide into two symmetrical limbs. There are 12 blades in the mix-flow rotor. The averaged inlet diameter of the rotor is 83.6mm and the cone angle is -40 degrees. The configurations of the turbine are shown in figure 1.

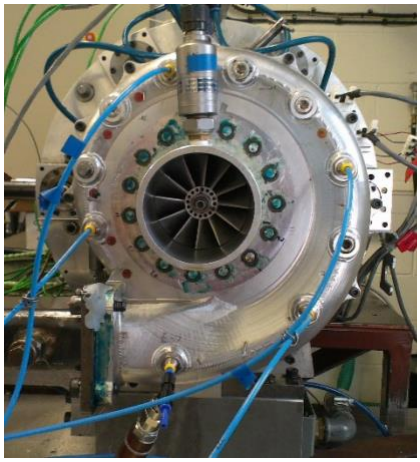

(a) mix-flow turbine

(b) nozzled volute

Figure 1. Mix-flow turbine for the investigation

Main geometrical parameters of the turbine are shown in table 1.

Table 1. Main geometrical parameters of the nozzled turbine

Geometries	Values
A/R(mm)	33.0
Number of nozzle vanes	15
Vane angle (deg)	60
Inlet mean diameter(mm)	83.6
Inlet blade height	18.0
Inlet blade angle (deg)	-20
Exit hub diameter(mm)	27.1
Exit tip diameter(mm)	78.6
Number of blades	12
Rotor blade length(mm)	40.0

The unsteady 3D CFD simulation is applied for the investigation via commercial software ANSYS-CFX. The volute is meshed by the tetrahedral element to obtain the good mesh quality, and there are 1.03 million elements in the twin-entry volute. The nozzle and the rotor are meshed by the hexahedral element via the TurboGrid. There are about 143k and 131k elements

in each nozzle passage and the rotor passage, respectively, which results in 2.14 million and 1.58 million elements in the nozzle and the rotor, respectively. The total number of the elements in computational domains of the twin-entry turbine is about 5.09 million. The distance of the first layer of mesh from solid walls is set to be 1×10^{-5}m, which results in a reasonably small averaged y^+ (the area averaged value is about 2.4). Moreover, the automatic wall treatment method is applied for near-wall treatment, which is adapted to the mesh size near the wall and hence reduces the sensitivity of the results on the y^+. The meshes of the turbine are presented in figure 2.

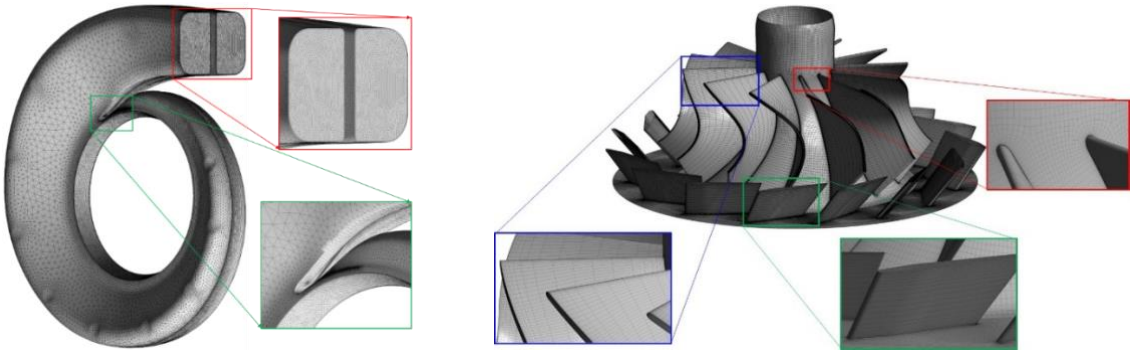

(a) volute (b) nozzle and rotor

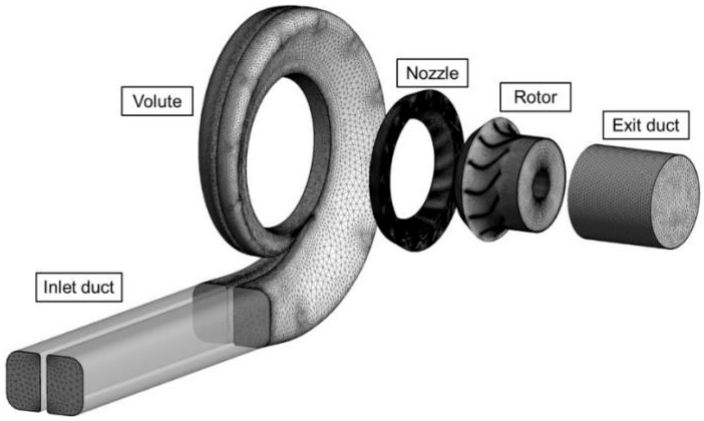

(c) computational domains

Figure 2. Meshes and computational domains of the turbine

Unsteady Reynolds Averaged Navier-Stokes equations (URANS) are applied as control equations. k-ω based Shear Stress Transport model (SST) is used to model the turbulence for the closure of control equations[17]. The high-resolution scheme is employed for spatial discretization. The physical time step of the iteration is set to be 1.38×10^{-5}s, which accounts for

4 degrees of the rotor rotation. It has been confirmed as a reasonable value to capture main flow structures in the turbine [18, 19]. The residual target of convergence criteria is set as 10^{-5} and the maximum steps of inner iteration are 10. Transient total pressure and total temperature from experiment, together with the velocity direction (normal to the inlet boundary) are imposed as inlet boundary conditions. Meanwhile, instant area-averaged static pressure from experiment is used as the outlet boundary condition. The transient rotor-stator method (sliding mesh) is applied for the treatment of the rotor/stator interface which locates in the middle of the nozzle and the rotor. In this method, the meshes of the rotor rotate at each physical time step during the calculation, and the transient interaction between the stator and the rotor can be considered reliable [20].

The CFD method is validated by experimental measurements which were carried out on the turbine test rig at Imperial College London. Detailed information about facilities and measurement methods are introduced in the literature [21]. Turbines with nozzled single-entry volute were tested for the validation at steady and pulsating conditions. Figure 3 compares the predicted performance with the experimental results under steady and pulsating inflow conditions with the pulse frequency of 60 Hz at 4.9 kRPM (80% design speed). It can be seen in subfigure (a) and (b) that the predicted hysteresis loops of both swallowing capacity and output torque are similar to experimental results. It is worth mentioning that the details of the loop at the head and tail are well predicted by the simulation, indicating the good capability of the prediction on detailed gas dynamic behaviours in the turbine. Moreover, the averaged discrepancy between the prediction and experiment is 5.3% and 3.1% for the swallowing capacity and the torque, respectively. It is considered to be a good accuracy referring to the results published in literature [22]. Therefore, the method is reliable for further investigations in this paper.

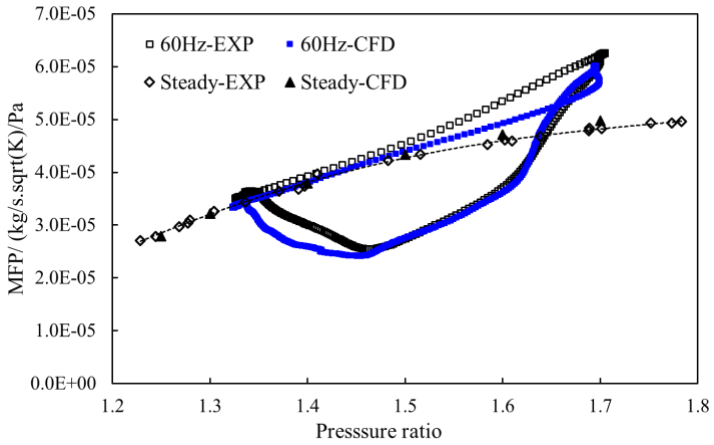

(a) swallowing capacity

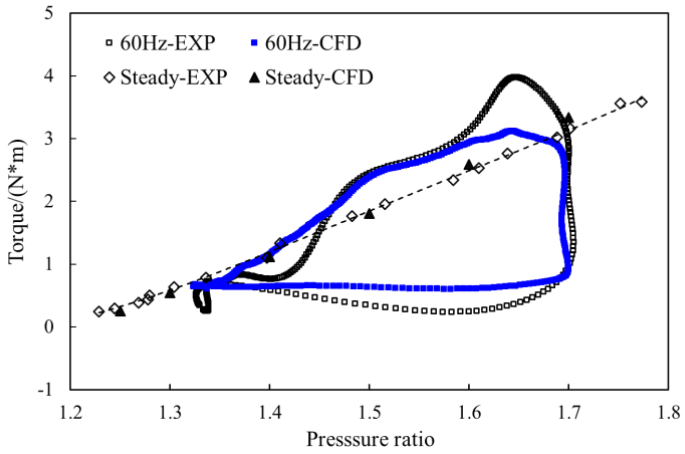

(b) output torque

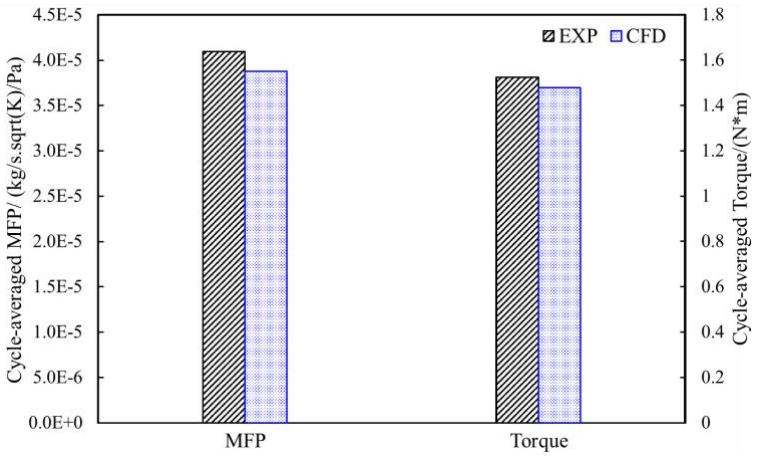

(c) cycle-average parameter

Figure 3. CFD validation for the turbine at pulsating conditions

Results Analysis

Definitions of turbine performance

Normally, flow conditions of two limbs of the twin-entry volute are evidently different under pulsating conditions because of the flow is fed in out-of-phase. Therefore, it is important to define reasonable parameters of the performance tailored for the pulsating conditions. Considering that the turbine is the component of energy converting, the performance is defined based on the energy-averaged method.

The equivalent total pressure, mass flow rate parameter (MFP) at instant time are calculated by the equivalent temperature and total pressure ratio, as given in equation (1) ~ (3).

Equivalent temperature:

$$T_{t-equi} = \frac{T_{t-hub} \cdot m_{hub} + T_{t-shr} \cdot m_{shr}}{m_{hub} + m_{shr}} \tag{1}$$

Equivalent pressure ratio:

$$T_{t-equi}(1 - PR_{equi}^{\frac{1-\gamma}{\gamma}})(m_{hub} + m_{shr}) = T_{t-hub}(1 - PR_{hub}^{\frac{1-\gamma}{\gamma}})m_{hub} + T_{t-shr}(1 - PR_{shr}^{\frac{1-\gamma}{\gamma}})m_{shr} \tag{2}$$

The equivalent mass flow rate parameter at instant time:

$$MFP_{equi} = m_{hub}\frac{\sqrt{T_{t-hub}}}{P_{t-hub}} + m_{shr}\frac{\sqrt{T_{t-shr}}}{P_{t-shr}} \tag{3}$$

The instant isentropic work of the two limbs:

$$\dot{W}_{is,hub} = C_p T_{hub} m_{hub}(1 - PR_{hub}^{\frac{1-\gamma}{\gamma}}) \tag{4}$$

$$\dot{W}_{is,shr} = C_p T_{shr} m_{shr}(1 - PR_{shr}^{\frac{1-\gamma}{\gamma}}) \tag{5}$$

In addition to the instant performance, cycle averaged performance over a pulse period is also defined for the comparison of overall performance under pulsating conditions. The cycle-averaged pressure ratio, mass flow rate parameter, and the efficiency are defined as equation (6) ~ (8).

Cycle-average pressure ratio:

$$\overline{PR}_{cyc} = \frac{\int_T \dot{W}_{is}(PR_{equi})_{inst}\,dt}{\int_T \dot{W}_{is}\,dt} \tag{6}$$

Cycle-average MFP:

$$\overline{MFP}_{cyc} = \frac{\int_T MFP_{equi,inst}\,dt}{T} \tag{7}$$

Cycle-average turbine efficiency:

$$\bar{\eta}_{cyc} = \frac{\int_T \dot{W}_{act}\,dt}{\int_T \dot{W}_{is}\,dt} = \frac{\int_T (\tau\omega)_{inst}\,dt}{\int_T \left(\dot{W}_{is,hub} + \dot{W}_{is,shr}\right)dt} \tag{8}$$

Turbine performance

The frequency is one of the most important characteristics of the pulse. In fact, the dimensionless coefficient Strouhal number, which is proportional to the frequency, is normally applied to evaluate the unsteadiness of the turbine [23, 24]. The definition of Strouhal number is as follows:

$$St = \frac{f \cdot L}{U} \tag{9}$$

Where f is the frequency, L and U are characteristic length and velocity, respectively.

This coefficient reflects the relationship between the time scale of pulse and its propagation. The system can be considered as the quasi-steady if the coefficient is small, while the unsteadiness can't be ignored if the coefficient is large. For the current study, L is fixed for the investigated turbine. The flow parameter U can't be manipulated conveniently. Therefore, the correlation of Strouhal number with the unsteadiness is studied by changing the pulse frequency.

Normally, it is difficult to isolate the influence of the pulse frequency from the pulse magnitude and shape in the experiment because the magnitude and shape are both strongly coupled with the frequency of the pulse. In order to study the influence of Strouhal number on the unsteadiness of turbine performance, the influencing factor of the frequency is isolated numerically via changing the frequency but with the same pulse magnitude and the shape. Three cases of pulsating inflow with different Strouhal number are applied, including 0.156 (f=20 Hz), 0.331 (f=40 Hz) and 0.522 (f=60 Hz). The instantaneous performance at St=0.156 and St=0.522 is plot and compared in figure 4. The performance at full admission and partial admission is also plot in the figure for the convenience of analysis. Subfigure (a) compares the instant MFP versus the pressure ratio. By scrutiny of the two loops with different Strouhal numbers, it can be observed that the hysteresis loop of swallowing capacity at St=0.156 is bounded by the steady turbine performance at full and partial admissions. However, a small portion of the loop for St=0.522 stretches out of the characteristic of full admission, clearly manifesting the stronger unsteadiness of the turbine performance. Similar phenomenon can be observed for the performance of output torque, as shown in subfigure (b). It is therefore inferred that the unsteadiness is enhanced as the Strouhal number increases. Moreover, different from the phenomenon in a single entry turbine, there are two main loops overlapped with each other for the twin-entry turbine, as shown in figure 4. This phenomenon is apparently caused by two out-of-phase pulses at the turbine inlet. The cycle-average performance is also shown in the figure

as the scattered square and triangle. It is observed that the averaged MFP for St=0.522 is 3.2% higher than that of St=0.156, while the averaged torques are approximately the same.

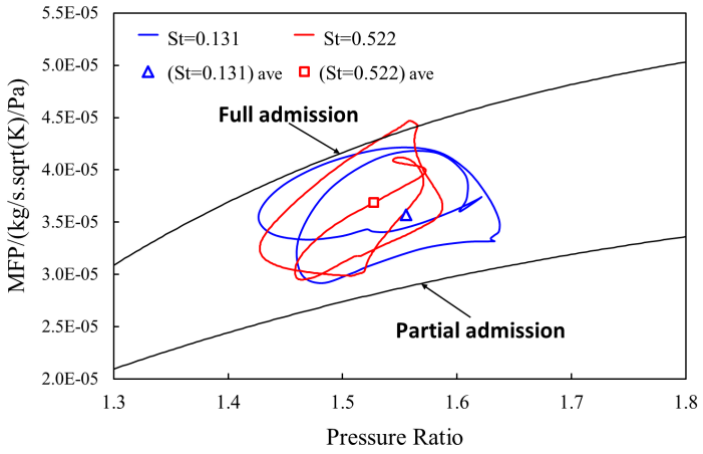

(a) swallowing capacity

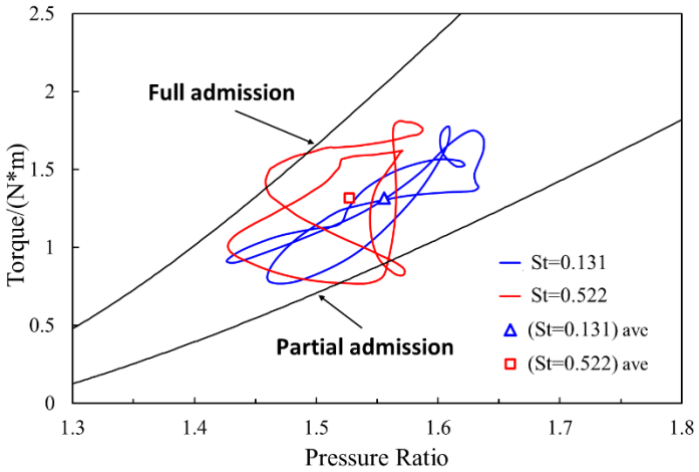

(b) output torque

Figure 4. Turbine performance under different Strouhal numbers

Figure 5 demonstrates the influence of Strouhal number on turbine performance including the cycle-average mass flow rate parameter and efficiency. The performance is normalized by the one at quasi-steady condition. Particularly, the case as St=0 is the corresponding quasi-steady cases when the turbine works in steady behaviours. Therefore, the deviation from the performance of quasi-steady is the direct indicator of the turbine unsteadiness at pulsating conditions. The correlation of unsteadiness of the turbine performance with Strouhal number is

clearly demonstrated in the figure. Importantly, it is observed that the discrepancies of turbine performance between the pulsating condition and quasi-steady condition increase evidently as Strouhal number increases. Specifically, when the Strouhal number is below 0.1, the discrepancies are less than 0.6%, thus the system can be reasonably considered as steady. This is in good accordance with the criteria proposed in previous researches. As St further increases to 0.522, MFP is about 3.5% higher and the turbine efficiency is about 3.4% higher than quasi-steady case. The turbine unsteadiness with twin-entry volute is notably enhanced by the increase of Strouhal Number. Interestingly, it is worth mentioning that the phenomena are opposite to turbine performance under pulsating inflow of single-entry turbine or double-entry turbine, where the performance under pulsating inflow is lower than that under quasi-steady condition [12].

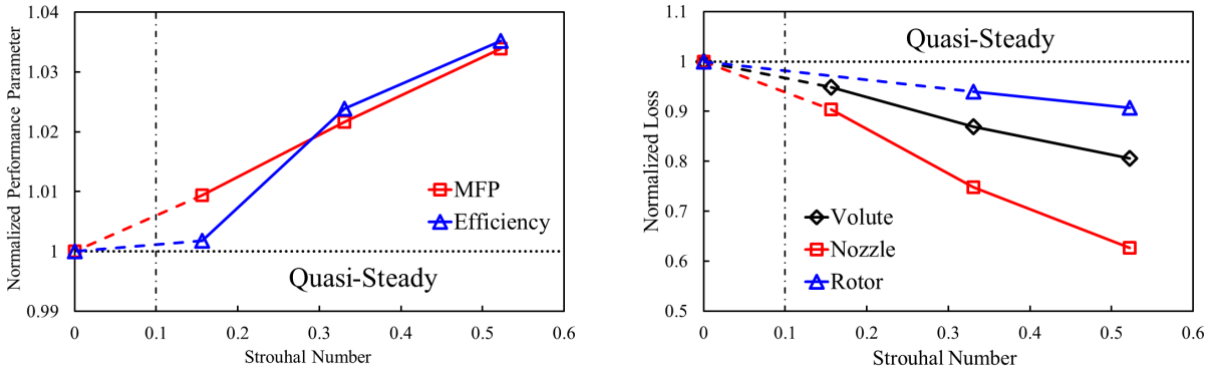

(a) normalized turbine performance (b) normalized loss in turbine

Figure 5. Normalized performance parameters under different Strouhal numbers

In order to allocate the reasons for the performance unsteadiness, detailed flow loss distribution in the turbine is evaluated. The method of loss evaluation at pulsating condition is going to be discussed in the following paragraphs. Figure 5(b) shows the influence of Strouhal number on the cycle-average loss of turbine components, including the volute, the nozzle and the rotor at pulsating inflows. Correlated with the turbine efficiency shown in figure 5(a), the loss in the three components under pulsating inflows is evidently lower than that under quasi-steady condition. Moreover, as Strouhal number increases, the loss in all the three components

decreases gradually. Importantly, it can be seen that the largest discrepancy of the loss between the quasi-steady and pulsating inflows appears in the nozzle, where the value is reduced to 0.626 at the case with St=0.522. The discrepancy of the loss in the rotor is the minimum at all conditions among three components. Therefore, it can be concluded that the nozzle is the component contributing the most to the unsteady behaviours of the turbine with twin-entry volute at pulsating conditions. On the other hand, the rotor is the most 'steady' component, which justifies the assumption of 'quasi-steady' for the turbine rotor in previous researches.

Furthermore, in addition to the cycle-average flow loss as shown in figure 5(b), the instantaneous flow loss of the turbine components is discussed. Entropy generation in the controlled volume is employed for the evaluation of the loss. For pulsating conditions, the entropy generation can't be evaluated by the convection of the parameter because the flow on the boundary of the volume is not at the same instant time. To evaluate the loss generation in a component at pulsating condition, the entropy generation rate in a unit volume is evaluated as equation (10).

$$\sigma=\int_V \frac{1}{\overline{T}}\left(\overline{\tau}_{ij}\frac{\partial \overline{u}_i}{\partial x_j}+\frac{\mu_t}{\mu}\overline{\tau}_{ij}\frac{\partial \overline{u}_i}{\partial x_j}\right)dv=\int_V \frac{\mu+\mu_t}{\mu\overline{T}}\overline{\tau}_{ij}\frac{\partial \overline{u}_i}{\partial x_j}dv \tag{10}$$

The instantaneous loss breakdown of three components in the turbine, including the volute, the nozzle and the rotor, under quasi-steady condition and two pulsating conditions (St=0.331 and 0.522) is demonstrated in figure 6. Subfigure (a) manifests the loss breakdown of three components at quasi-steady condition (St=0). The pressure at the entries of two limbs is superimposed in the figure. By the scrutiny of the pulsations in the figure, it can be observed that the loss in all three components fluctuates with pulsating inlet conditions. In general, the higher the pressure is, the more the loss is generated in three components. Importantly, the loss in the nozzle is the most strongly influenced by the inlet conditions, followed by the rotor and the volute. Specifically, the peak loss happens at '*A*' and '*B*' which correspond to the two partial

admission conditions during a pulse period, as shown in subfigure (a). This is in accordance with the phenomenon observed in steady conditions [25]. The highest loss and hence lowest efficiency tends to happen at partial admission conditions because of strong mixing loss and highly distorted flow in spanwise direction at inlet of the rotor. According to the pulse of pressure, at time '*A*' is the partial admission when the maximum portion of flow is fed to the limb near shroud side. At the meantime, at time '*B*' is the admission when the flow is mainly fed to the hub side.

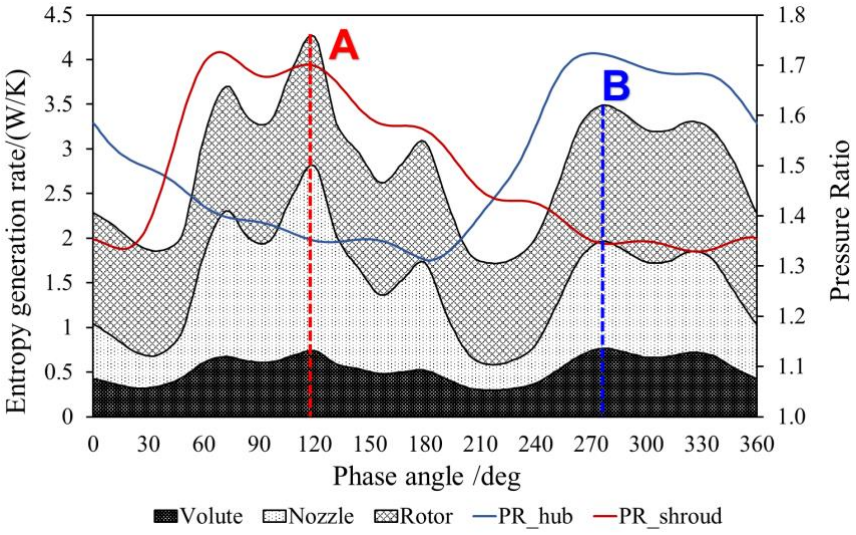

(a) St=0 (quasi-steady)

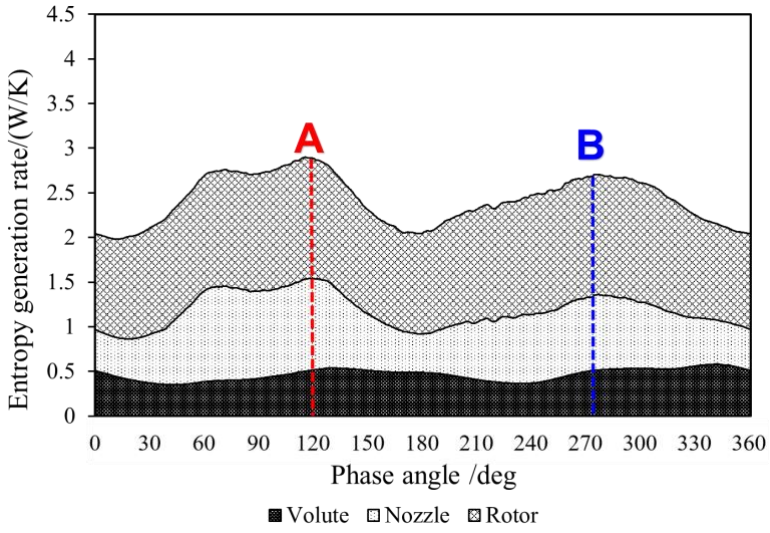

(b) St=0.331(40Hz)

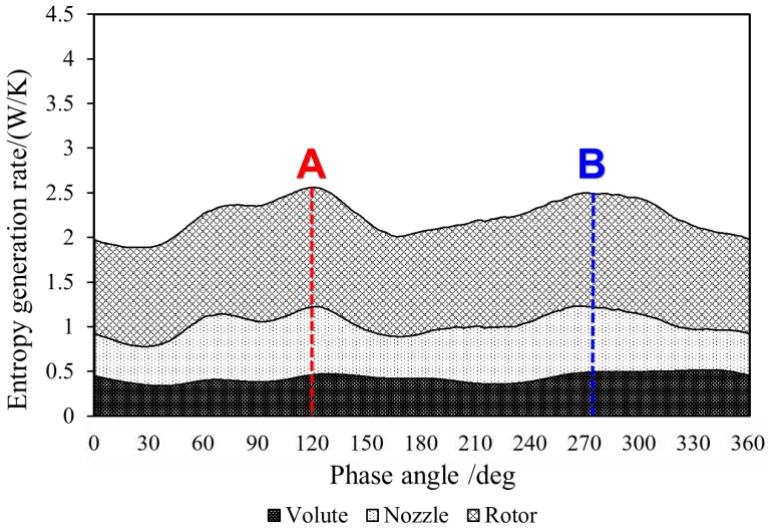

(c) St=0.522(60Hz)

Figure 6. The normalized entropy generation rate of the turbine

Subfigure (b) and (c) manifest the instantaneous loss breakdown in the turbine at pulsating conditions with two Strouhal numbers (0.331 and 0.522). Because it takes time for a pulse to propagate from the turbine inlet to the exit, there is evident phase difference among the flow parameters throughout the turbine. The instantaneous loss in different components at pulsating conditions can't be compared intuitionisticly. Therefore, in order to compare conveniently the loss breakdown at different pulsating conditions, phase shift method is employed on the loss analysis in the turbine components. The average sonic speed plus the bulk flow velocity are applied for the phase shift, which is proposed in previous researches [26]. Two important facts can be observed in figure 6 (b) and (c). Firstly, the fluctuations of the loss in all three components become weaker notably at two pulsating conditions compared with quasi-steady case, especially for the nozzle. It is inferred that the response of flow parameters in the turbine is damped effectively at pulsating conditions with higher Strouhal number. Specifically, the magnitude of the fluctuations reduces by 81.1% as Strouhal number increase from 0 to 0.522. Secondly, the loss reduces evidently in the nozzle compared with the quasi-steady case (subfigure (a)). Moreover, the reduction is further enhanced at higher Strouhal number. Similar trend can be seen in the volute, although the magnitude is smaller. At the meantime, there is no notable variation of loss appears in the rotor. This phenomenon is in high accordance with the

loss variation demonstrated in figure 5 (b). It can be concluded that the unsteadiness of the turbine performance with twin-entry nozzled volute is mainly contributed by the unsteady performance of the nozzle. Furthermore, the unsteady performance of the component is significantly depressed by increase of Strouhal number.

Flow analysis

According to the loss breakdown comparison of turbine at different conditions, it is concluded that the flow in the nozzle is the key for the turbine unsteady behaviours. In order to understand the influence of Strouhal number on the unsteady performance of turbine, detailed flow field in the nozzle is discussed in the following sections.

For a twin-entry turbine, the flow in the two limbs of the volute is different at most of the time during a pulsating condition due to out-of-phase pressure pulses imposed on the two entries, as indicated in figure 6. Consequently, the flow field at inlet of the nozzle is highly distorted during the pulsating conditions, which then directly influences the flow in the nozzle. Figure 7 demonstrates the variation of circumferentially averaged flow angle at nozzle inlet at two pulsating conditions with different Strouhal numbers (St=0 and St=0.522). Subfigure (a) shows the flow angle at quasi-steady conditions (St=0). It is observed that the flow distribution in spanwise direction is highly distorted at the condition. Moreover, the distribution of the flow angle in spanwise direction varies with the time significantly. There are two peaks of the flow angle ('*PA*' and '*PB*') during the pulse period which is in accordance with the locations of two peak values of pressure pulses ('*A*' and '*B*') at the turbine inlet. When the pulse period is between 50 to 180 degrees, low pressure is imposed at the limb near hub side, and hence produces higher flow angle at the low portion of spanwise near the hub side, as shown in the subfigure (a). The dark blue region at the vicinity of the hub is considered to be resulted from the boundary layer nearby. On the other hand, in the region between 180 to 360 degrees, high flow angle is produced near shroud side because the pressure imposed on the limb near shroud

is low. Specifically, there is a considerably large region near the shroud in this region ('*PB*') with the flow angle higher than 90 degrees, indicating that there is strong reverse flow. Subfigure (b) manifests the flow angle evolution at St=0.522. It can be immediately observed that the fluctuations of the flow angle are much gentler during the pulse period, although the distribution pattern is approximately similar to the one at St=0 shown in subfigure (a). Specifically, the magnitude of the flow angle variation at St=0.522 reduces by more 50%. Compared subfigure (a) and (b), it is concluded that the fluctuations of flow angle at the inlet of the nozzle are effectively damped by the increase of Strouhal number. Since the flow field in the nozzle is heavily depended on the inlet flow condition, the detailed flow in the nozzle is expected to be influenced by the damping effect.

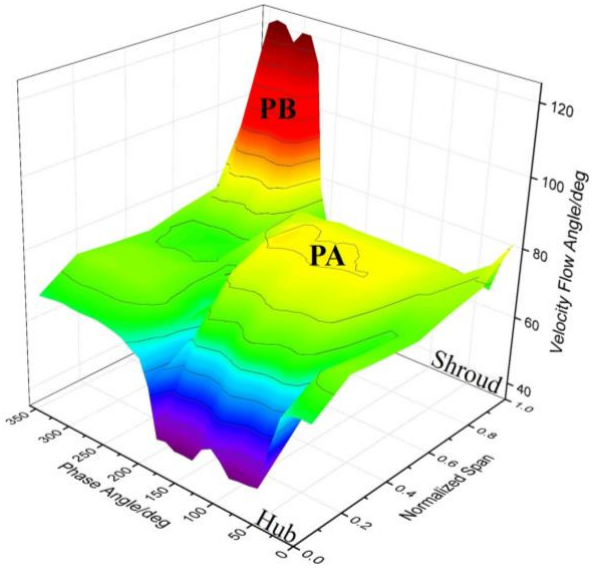

(a) St=0 (quasi-steady condition)

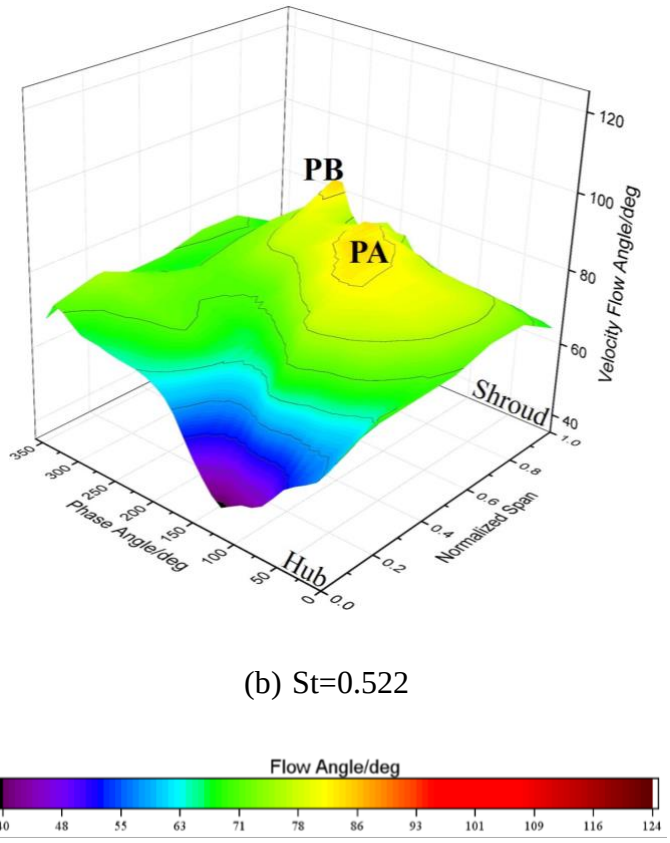

(b) St=0.522

Figure 7. Distribution of flow angle at the inlet of nozzle

Figure 8 demonstrates the evolution of the vortex structures in the nozzle passage during a pulse period at St=0.331 (*f*=40 Hz). The structure is plotted via λ_2 criterion which is capable of showing the core of the vortex [27]. In order to correlate the loss with the flow structures, the contours of the reduction of total pressure relative to the value at the nozzle inlet are manifested on the structures. Red colour indicates higher flow loss. Four instant times (t_1~t_4) are chosen for the investigation as shown in subfigure (a). Specifically, t_1 and t_3 represent two times with valley values of the loss in nozzle. At the meantime, t_2 and t_4 represent two times with peak values of the loss. For the convenience of analysis, the two peaks t_2 and t_4 are referred as case *A* and case *B*, respectively. At the time t_1, the flow is fed into the rotor approximately uniformly in spanwise direction. There is a weak horseshoe vortex in the shroud region near leading edge of the nozzle. Moreover, flow separation with small size but in red colour can be observed on the suction surface slightly downstream the leading edge. As the pulse runs to the time t_2, the inlet mass flow rate of the nozzle considerably increases compared with that at t_1, but is mainly

fed near the upper part of the blade near shroud region. Both the horseshoe vortex and the flow separation are enhanced evidently indicated by the much larger sizes due to large incidence angle and high flow velocity. Moreover, an evident horseshoe vortex also appears on the hub due to the poor inlet flow condition at lower part of the blade height, as shown in subfigure (c). Similar flow phenomenon to t_1 happens at t_3 when the horseshoe vortex and separation flow become weak because of the similar inlet flow condition of the nozzle. As the pulse further runs to t_4, the flow rate increases again but the majority of the flow is concentrated near the hub region. The flow separation on upper part of the suction surface disappears completely because little flow impinges with the leading edge of nozzle vane near shroud. On the other hand, there is strong reverse flow appearing at vicinity of the nozzle inlet in the shroud region. By the scrutiny of the colour on the vortex, it can be inferred that the flow separation, horseshoe vortex and reverse flow are the main contributors to the loss in the nozzle in all the instant times. As the pulse runs with time, these three sources of loss are generated, developed and disappear continuously responding to the variation of inlet flow condition. The evolution of the vortex structures results in the variation of the loss in the nozzle during the pulse period.

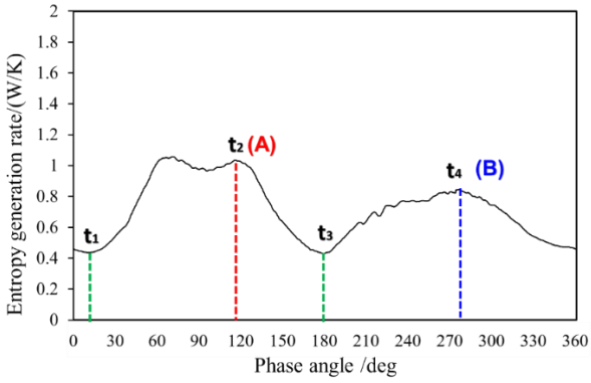

(a) time step

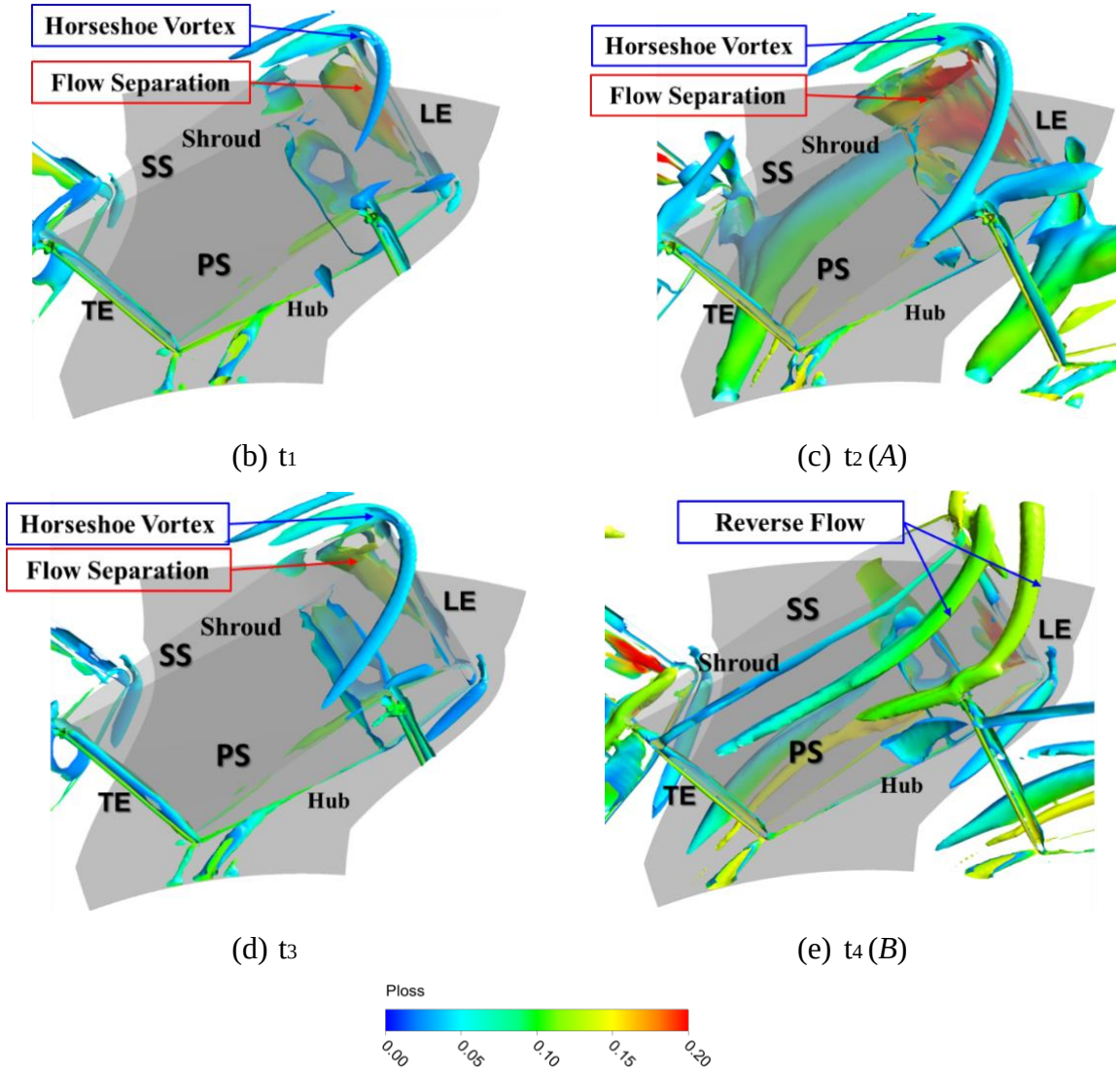

Figure 8. Flow field in nozzle through time under pulsating inflows (St=0.331)

Figure 9 compares the variation of vortexes in the nozzle at three Strouhal numbers for two the peaks of loss ('*A*' and '*B*' shown in figure 8(a)). Similar as the flow phenomenon in figure (8), the main flow patterns relating to the high loss in the nozzle for all the cases are the flow separation on suction surface, horseshoe vortex, and reverse flow near shroud region. However, the evolution of the flow structures with Strouhal number can be clearly observed in the figure. For the point '*A*' when the majority of flow is fed near the shroud region, the horseshoe vortex at shroud and hub shrinks as the Strouhal number increases from 0 (quasi-steady) to 0.522. Furthermore, the flow separation on suction surface is alleviated significantly, indicated by the smaller size and decay of the colour. For the point '*B*' when the majority of flow is fed to the

limb near the hub side, the vortex of reverse flow appears near the shroud region due to the large incidence angle near the shroud at St=0, as discussed above in figure 8. As St increases to 0.331, the reverse flow becomes weaker gradually, indicated by the size of the vortex as shown in figure 9 (b). As St further increases to 0.522, only the reverse flow with much smaller size can be seen in the nozzle, as shown in figure 9(d). According to the variation of the flow structures in the nozzle, it is concluded that the secondary flow with high loss is depressed by the increase of Strouhal number.

The alleviation of the secondary flow in the nozzle by the pulsating condition is resulted from two reasons. Firstly, the unsteady flow distortion at the nozzle inlet is depressed at the pulsating condition. The generation and development of the secondary flow in the nozzle are heavily depended on the inlet flow condition. As demonstrated in figure 7, the flow angle variation in spanwise direction at the nozzle inlet during a pulse period becomes much gentle as the Strouhal number increases from 0 to 0.522. Consequently, the deviation of the incidence angle from the average value is reduced and the generation of secondary flow such as flow separation and reverse flow can be depressed effectively. In fact, the alleviation of the flow fluctuations at the volute exit is caused by the twin-entry volute. Because there is a large volume in the volute, the pulsating incoming flow is well damped in the chamber before it propagates to the volute exit. Moreover, the higher the pulse frequency (also Strouhal number) is, the stronger damping effect is. Secondly, the development of the secondary flow in the nozzle is well depressed at pulsating condition. After the secondary flow is generated in the nozzle, it takes time to be fully developed. When the nozzle is fed by highly pulsating incoming flow, the environment for the development of flow structure varies quickly in the time. As a result, there is no enough time for the flow structures with high loss to be fully developed under the unsteady condition, which can be analogue to the ‘damping effect’ on the secondary flow. Moreover, the quicker the inflow changes, the stronger damping effect happens.

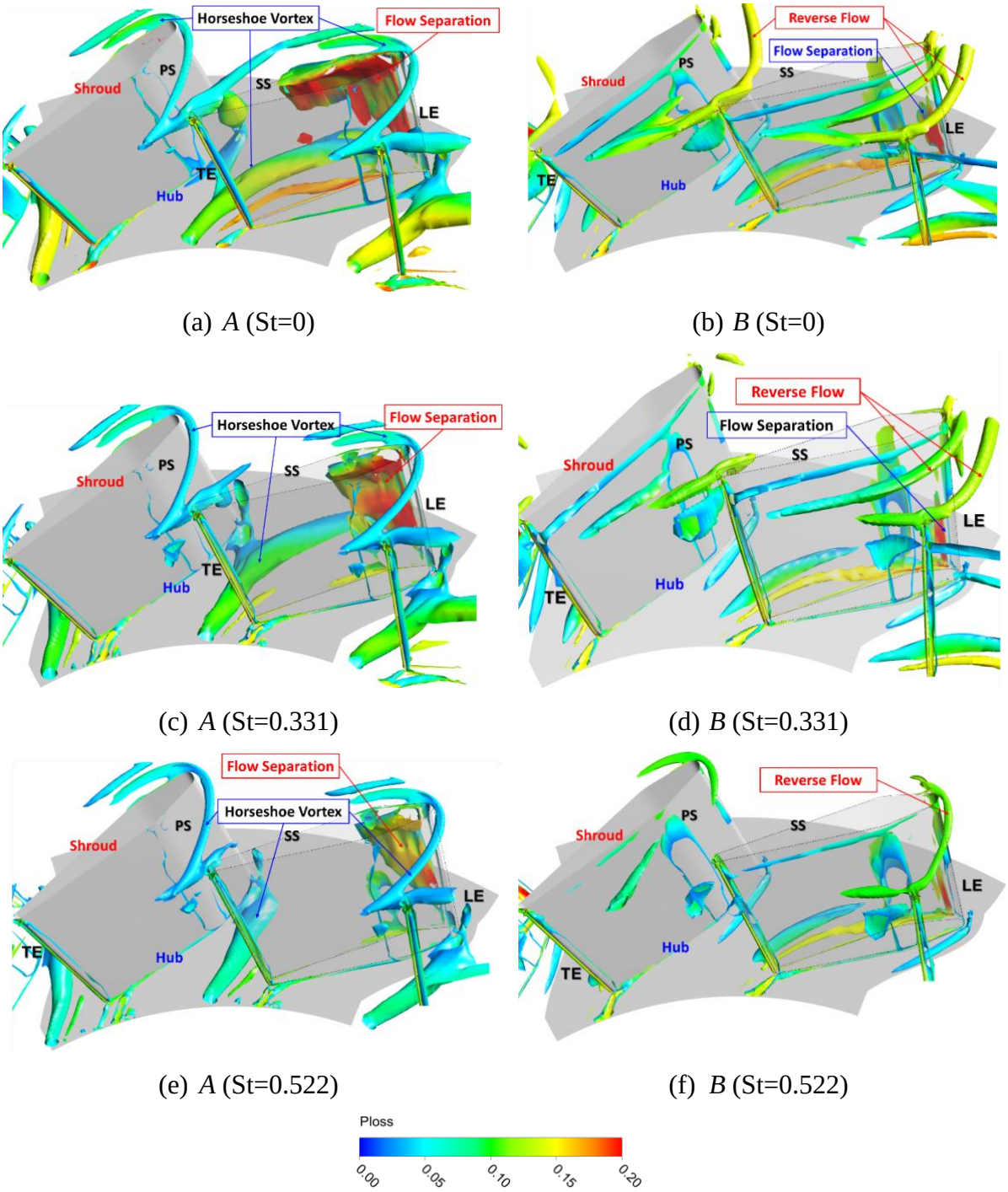

(a) *A* (St=0) (b) *B* (St=0)

(c) *A* (St=0.331) (d) *B* (St=0.331)

(e) *A* (St=0.522) (f) *B* (St=0.522)

Figure 9. Influence of St on vortex structure in nozzle at two instant times

Figure 10 further shows the distribution of entropy generation in nozzle passage for the time '*A*' and '*B*' at three Strouhal numbers. Three cross-section surfaces normal to streamwise direction are chosen for the analysis from the inlet to the outlet of the nozzle. For the time '*A*', there is a region with high entropy generation in all three sections near suction surface at St=0. Apparently, this region is in accordance with the strong flow separation as discussed in figure

9. As Strouhal number increases, the region shrinks consistently and can only be observed in the first section near the inlet at St=0.522. At the meantime, there is a region with high entropy generation in the hub corner, which corresponds to the large horseshoe vortex nearby, as shown in figure 9. This flow structure also decays quickly as Strouhal number increases. This confirms that the loss reduces significantly as St increases at the time '*A*'. For the point '*B*', there is a large region with notably high entropy generation near the shroud of the passage at St=0, which is in accordance with the reverse flow nearby. At the meantime, the region with high entropy generation can be seen near the suction surface as well as the hub corner. They are corresponding to the flow separation and horseshoe vortex near the hub region, as discussed in figure 9. As Strouhal number increases, all the regions with high entropy generation shrink and decay obviously, proving the reduction of loss in the nozzle. In conclusion, the alleviation of the secondary flow in the nozzle effectively reduces the flow loss in the nozzle at pulsating condition.

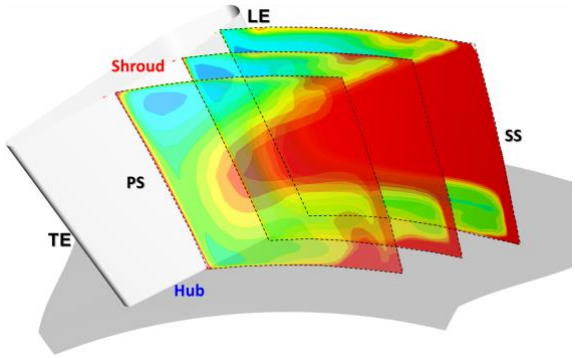

(a) *A* (St=0)

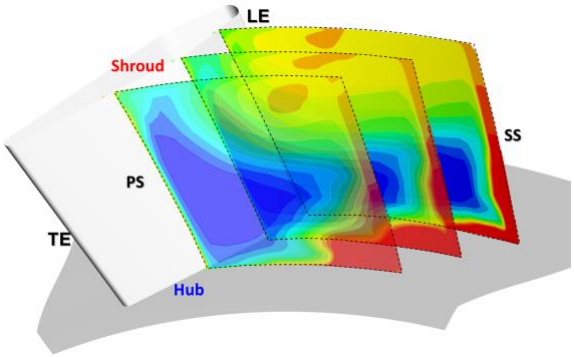

(b) *B* (St=0)

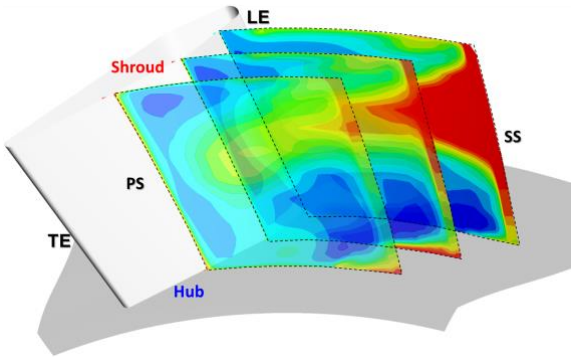

(c) *A* (St=0.331)

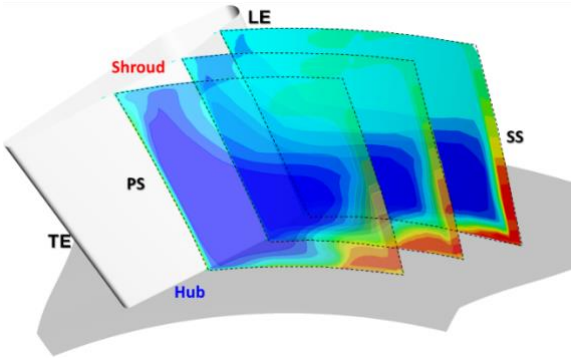

(d) *B* (St=0.331)

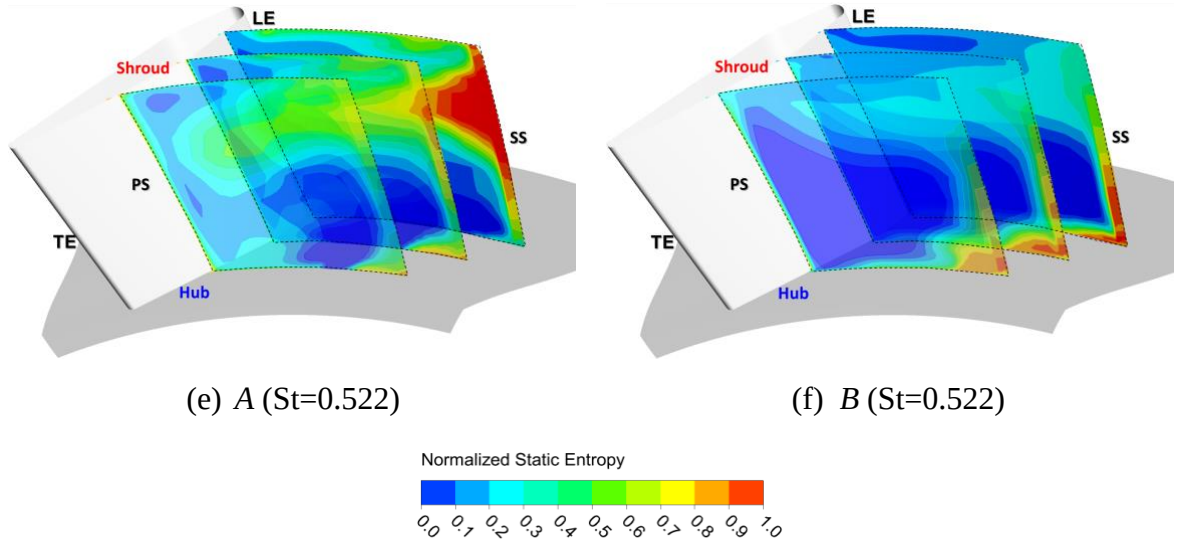

(e) *A* (St=0.522) (f) *B* (St=0.522)

Figure 10. Influence of St on entropy generation in nozzle at two instant times

By the scrutiny of entropy distribution in figure 10, it is observed that the scale of the regions with high entropy shrinks evidently as they are convected towards nozzle exit. It implies that the flow distortion caused by the twin-entry volute is alleviated as it moves downstream in the nozzle. Similar phenomenon has been observed in previous research [25]. The acceleration of flow is capable of depressing the development of the inlet flow distortion. As a result, the flow distribution at the inlet of the rotor, which is downstream the nozzle, is expected to be more uniform for all cases. Figure 11 compares relative flow angle distributions at the inlet of the rotor over a pulse period at quasi-steady (St=0) and pulsating conditions (St=0.522). Different from remarkable discrepancies at the nozzle inlet for the two cases, both the distribution and the magnitude of the flow parameters are similar. The minimum flow angle appears between 200~300 degrees near the hub side, which is in accordance with the distribution at the nozzle inlet. Specifically, the magnitudes of the fluctuations at the inlet and the exit are 54 degrees and 52 degrees, respectively.

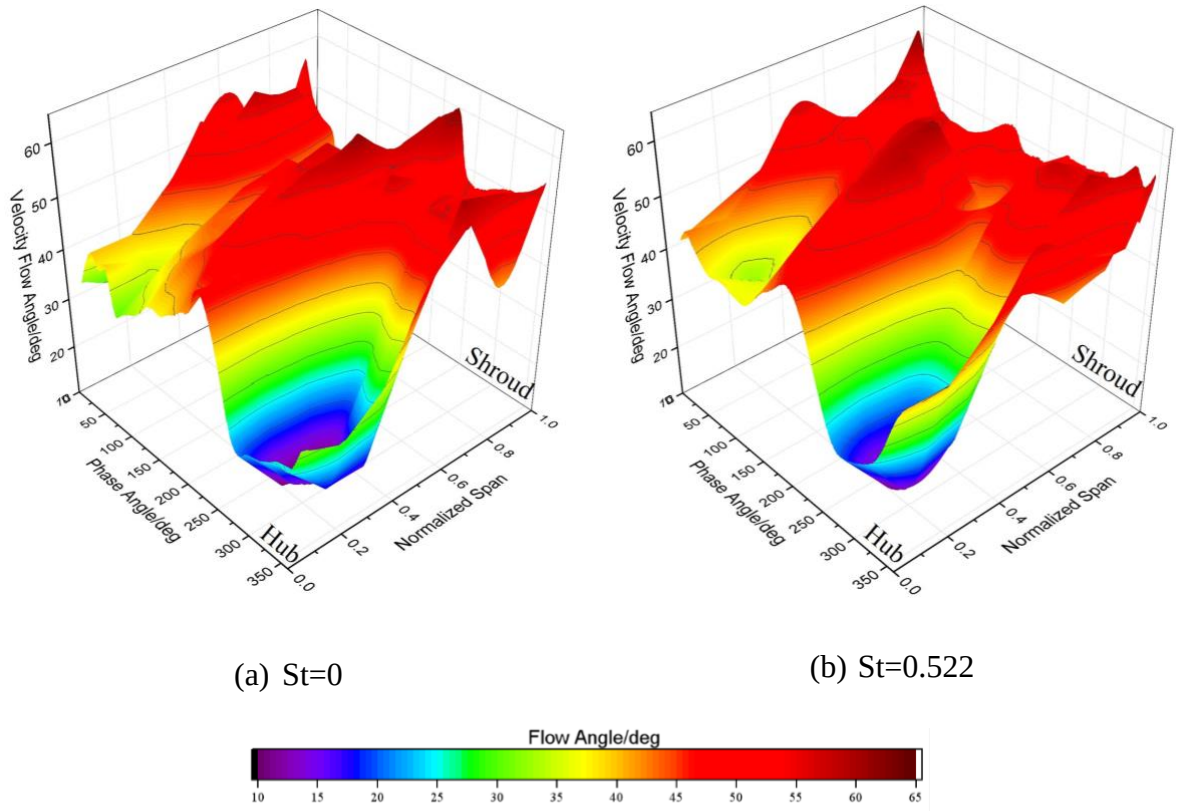

(a) St=0 (b) St=0.522

Figure 11. Distribution of flow angle at inlet of rotor

In order to quantitatively demonstrate the effects of distortion alleviation by pulsating condition, figure 12 further manifests discrepancies of the flow angle between quasi-steady (St=0) and pulsating inflow (St=0.522) at the inlet and outlet of the nozzle. Specifically, the positive value means that the flow angle at quasi-steady condition is larger, while negative value means the opposite situation. For the inlet of the nozzle, the main discrepancy between two cases is concentrated near the shroud in phase angle range as 250~360 degrees (zone-*A*). The maximum value is about 58.2 degrees. According to the flow field discussed previously, this region corresponds to the strong reverse flow near the shroud at the quasi-steady condition, but cannot be observed in the pulsating condition (St=0.522), as figure 9 shown. In addition, the flow angle in the middle blade height over phase angle 120~160 degrees (zone-*B*), the flow angle of quasi-steady condition is higher, which accounts for the larger scale of the flow separation in the nozzle. For the outlet of the nozzle, the discrepancies between two cases are much more uniform compared with the one at the inlet, clearly indicating a more effective alleviation on

the flow distortion at the pulsating condition. Specifically, the maximum discrepancy of flow angle reduces by 56.5%.

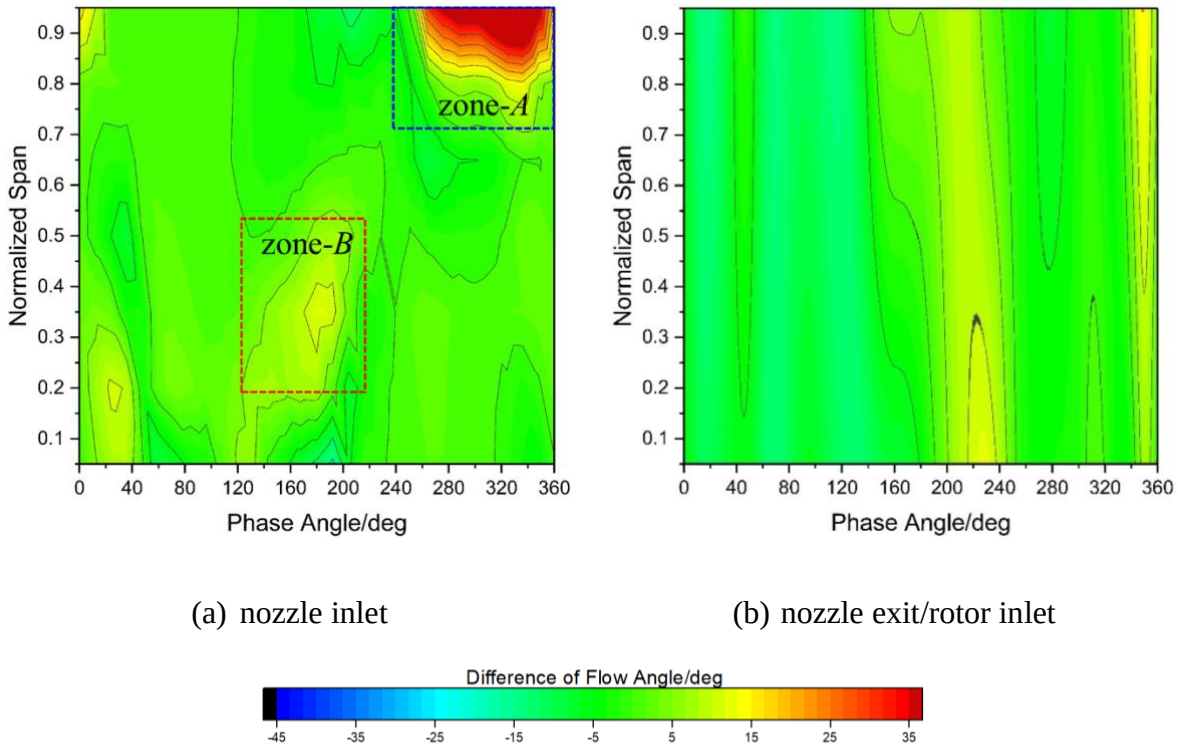

(a) nozzle inlet (b) nozzle exit/rotor inlet

Figure 12. Difference of flow angle between quasi-steady and pulsating inflows at the inlet and exit of nozzle

The depression of flow distortion at nozzle exit by pulsating condition inevitably influences the flow evolution in the rotor. Figure 13 compares the pattern of streamlines threading through the regions with high entropy generation in a rotor passage of at the time '*B*' for two Strouhal numbers (St=0 and St=0.522). For St=0, hub separation is generated at about 50% chord length and then a strong vortex rolls up near the suction surface. Furthermore, the flow structure of hub separation is in accordance with the high entropy generation region as the contours shown in the figure. At the meantime, strong tip leakage vortex is initiated at 40% chord length and then migrates to the rotor exit near the shroud. This vortex structure also contributes to the high entropy generation, as indicated by contours in red colour. Similar flow patterns have been observed in previous studies and they are confirmed to be main source of loss in the rotor passage [25]. For the pulsating condition as St=0.522, same flow features in the rotor are

observed in the pulsating inflow condition with slightly weaker vortexes indicated by their size. The flow patterns in the turbine rotor are similar between the quasi-steady and pulsating conditions.

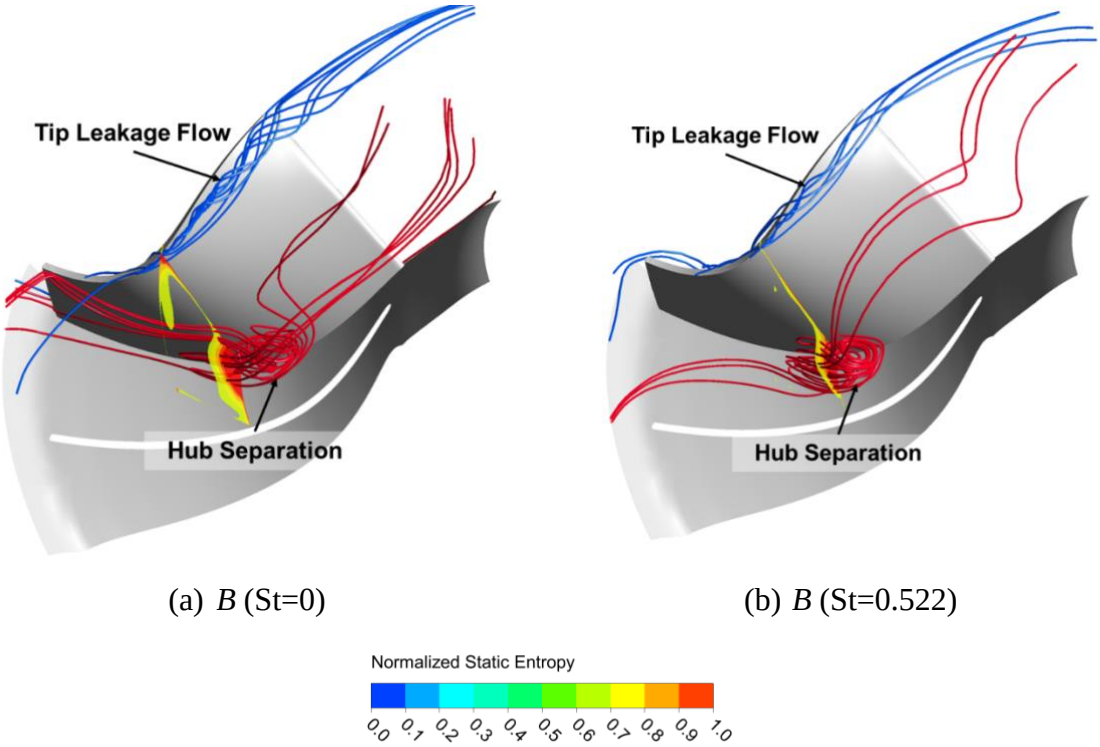

(a) *B* (St=0) (b) *B* (St=0.522)

Figure 13. Flow field in the rotor at quasi-steady/pulsating inflow at time '*B*'

According to the comparison of flow structures in the rotor, it can be concluded that the damping effect of the nozzle on the unsteady flow distortion at pulsating conditions for a twin-entry turbine results in a less 'unsteady' rotor. This is in high accordance with the loss characteristics of the rotor at different pulsating conditions as demonstrated in figure 5 and 6.

Conclusions

Twin-entry turbine of a turbocharger is confronted by pulsating inflows due to the firing sequence of the internal combustion engine. This paper studies the performance as well as flow mechanism of a twin-entry nozzled mix-flow turbine under pulsating inflows via experimental validated numerical method. Four main conclusions are drawn as follows:

(1) The performance of the mixed flow turbine with nozzled twin-entry volute is studied at pulsating inflows with different Strouhal numbers. It is found that Strouhal number has a notable influence on turbine performance. Moreover, the turbine performance increases consistently at Strouhal number increases, manifesting that the unsteadiness of the performance of the twin-entry turbine is enhanced by the pulsating inflows. Specifically, cycle-average mass flow parameter and efficiency of the pulsating inflows with St=0.522 is 3.5% and 3.4% higher than that of the quasi-steady condition (St=0), respectively;

(2) The loss breakdown of the components in the turbine has been analysed at different Strouhal number. The results show that the nozzle is the main contributor to the unsteadiness of the performance at pulsating conditions. In particular, the loss in the nozzle is decreased significantly by 37.3% at St=0.522 than that at St=0. On the other hand, the loss in the rotor is relatively lower (~9%) for the pulsating inflows;

(3) Flow analysis in the nozzle shows that the secondary flow, including the flow separation on suction surface, the reverse flow near shroud and horseshoe vortexes, are the main sources of flow loss in the nozzle. Compared with the quasi-steady condition, the scale of these flow structures is evidently smaller under pulsating inflows condition, hence the loss in the pulsating inflows is lower;

(4) The alleviation of the secondary flow in the nozzle is resulted from two reasons. One is the depressing of flow distortion at nozzle inlet resulted from the damping effect of the twin-entry volute on the pulsating incoming flow. The other is the damping effect on the development of the secondary flow inside the nozzle because of the delay of the response of the flow structures to the fast-varying inlet flow conditions. Moreover, the nozzle further alleviates the flow distortion at the inlet of the turbine rotor, resulting in similar flow patterns in the rotor between quasi-steady and pulsating conditions.

Acknowledgements

This research is supported by Natural Science Foundation of China (NSFC) (Grant No. 51606121).

References

[1] Pescini E., Giorgi M., Suma A., Francioso L., and Ficarella A.. Separation Control by a Microfabricated SDBD Plasma Actuator for Small Engine Turbine Applications: Influence of the Excitation Waveform. Aerospace Science and Technology, 2018; 76: 442-454.

[2] Winkler N., Ångström H., and Olofsson U.. Instantaneous On-Engine Twin-Entry Turbine Efficiency Calculations on a Diesel Engine. SAE Technical Paper, 2005; 2005-01–3887.

[3] Schorn N. A.. The Radial Turbine for Small Turbocharger Applications: Evolution and Analytical Methods for Twin-Entry Turbine Turbochargers. SAE International Journal of Engines, 2014; 7(3):1422-1442.

[4] Lymberopoulos N., Baines N. C., and Watson N.. Flow in Single and Twin Entry Radial Turbine Volutes. ASME Paper, 1988; 88-GT-59.

[5] Romagnoli A., Martinez-Botas R. F., and Rajoo S.. Steady State Performance Evaluation of Variable Geometry Twin-Entry Turbine. International Journal of Heat and Fluid Flow, 2011; 32 (2): 477–489.

[6] Liu Y. K., Yang M. Y., Deng K. Y., Chen H., and Martinez-Botas R. F.. Design and Flow Mechanism Analysis of Radial Turbine with Twin-entry Volute. Vehicle Engine, 2017; 1:8-13.

[7] Costall A. W., McDavid R. M., Martinez-Botas R. F., and Baines N. C.. Pulse Performance Modeling of a Twin Entry Turbocharger Turbine under Full and Unequal Admission. Journal of Turbomachinery, 2011; 133:021005-1-8.

[8] Palenschat T., Newton P., Martinez-Botas R. F., Müller M., and Leweux J.. 3-D Computational Loss Analysis of an Asymmetric Volute Twin-scroll Turbocharger. Proceedings of ASME Turbo Expo, 2017; GT2017-64190.

[9] Rajoo S., Romagnoli A., and Martinez-Botas R. F.. Unsteady Performance Analysis of a Twin-entry Variable Geometry Turbocharger Turbine. Energy, 2012; 38:176-89.

[10] Yang M., Deng K., Martinez-Botas R. F., and Zhuge W.. An Investigation on Unsteadiness of a Mixed-flow Turbine under Pulsating Conditions. Energy Conversion and Management, 2016; 110: 51-58.

[11] Szymko S., Martinez-Botas R. F., and Pullen K. R.. Experimental Evaluation of Turbocharger Turbine Performance under Pulsating Flow Conditions. Proceedings of ASME Turbo Expo, 2005; GT2005-68878.

[12] Copeland C. D., Martinez-Botas R. F., and Seiler M.. Comparison between Steady and Unsteady Double-entry Turbine using the Quasi-steady Assumption. Journal of Turbomachinery, 2011; 133: 031001.

[13] Copeland C. D., Seiler M., and Martinez-Botas R. F.. Unsteady Performance of a Double Entry Turbocharger Turbine with a Comparison to Steady Flow Conditions. Journal of Turbomachinery, 2012; 134: 021022.

[14] Copeland C. D., Newton P., Martinez-Botas R. F., and Seiler M.. The Effect of Unequal Admission on the Performance and Loss Generation in a Double-Entry Turbocharger Turbine. Proceedings of the ASME Turbo Expo, 2010; GT2010-22212.

[15] Cerdoun M., and Ghenaiet A.. Unsteady Behaviour of a Twin Entry Radial Turbine under Engine Like Inlet Flow Conditions. Applied Thermal Engineering, 2018; 130 (2018):93-111.

[16] Yokoyama T., Hoshi T., Yoshida T., and Wakashima K.. Development of Twin-Entry Scroll Radial Turbine for Automotive Turbochargers using Unsteady Numerical Simulation. 11th International Conference on Turbochargers and Turbocharging, 2014: 471-478.

[17] Gao J., Wei M., Fu W., Zheng Q., and Yue G.. Experimental and Numerical Investigations of Trailing Edge Injection in a Transonic Turbine Cascade. Aerospace Science and Technology, 2019; 92 (2019): 258-268.

[18] Broatch A., García-Tíscar J., Roig F., and Sharma S.. Dynamic Mode Decomposition of the Acoustic Field in Radial Compressors. Aerospace Science and Technology, 2019; 90 (2019): 388-400.

[19] Padzillah M. H., Rajoo S., Yang M., and Martinez-Botas R. F.. Influence of Pulsating Flow Frequencies towards the Flow Angle Distributions of an Automotive Turbocharger Mixed-flow Turbine. Energy Conversion and Management, 2015; 98:449-462.

[20] Newton P., Martinez-Botas R. F., and Seiler M.. A Three-Dimensional Computational Study of Pulsating Flow Inside a Double Entry Turbine. Journal of Turbomachinery, 2014; 137: 031001-1-10.

[21] Yang M., Martinez-Botas R. F., and Rajoo S.. Influence of Volute Cross-Sectional Shape of a Nozzleless Turbocharger Turbine under Pulsating Flow Conditions. Proceedings of ASME Turbo Expo, 2014; GT2014-26150.

[22] Newton P. J.. An Experimental and Computational Study of Pulsating Flow within a Double Entry Turbine with Different Nozzle Settings. London: Department of Mechanical Engineering, Imperial College London, UK, 2013.

[23] Copeland C. D., Newton P., Martinez-Botas R. F., and Seiler M.. A Comparison of Timescales within a Pulsed Flow Turbocharger Turbine. 10th International Conference on Turbochargers and Turbocharging, 2012; 389-404.

[24] Cao T., Xu L., Yang M., and Martinez- Botas R. F.. Radial Turbine Rotor Response to Pulsating Inlet Flows. Journal of Turbomachinery, 2013; 136(7): 071003-1-10.

[25] Xue Y., Yang M., Martinez-Botas R. F., Romagnoli A., and Deng K.. Loss Analysis of a Mix-Flow Turbine with Nozzled Twin Entry Volute at Different Admissions. Energy, 2019; 166:775-788.

[26] Padzillah, M. H., Rajoo S., and Martinez-Botas R. F.. Numerical Assessment of Unsteady Flow Effects on a Nozzled Turbocharger Turbine. Proceedings of ASME Turbo Expo, 2012; GT2012-69062.

[27] Pátý M., and Lavagnoli S.. A Novel Vortex Identification Technique Applied to the 3D Flow Field of a High-Pressure Turbine. Proceedings of ASME Turbo Expo, 2019; GT2019-90462.